

## Supporting Information

**3D Printed hybrid Aerogel Gauzes Enable Highly Efficient Hemostasis**

*Xiaoxu Yang, Nan Shi, Jian Liu, Qingqing Cheng, Guangyong Li, Jing Lyu, Fengguo Ma\*, Xuotong Zhang\**

**1. Calculation of the extrusion speed of KNF-PVA inks**

The governing equation of the pressure-driven laminar flow of KNF-PVA inks reads as

$$\frac{\partial P}{\partial z} = \frac{1}{r} \frac{\partial}{\partial r} (r \tau_{rz}) \quad (1)$$

where  $r$  and  $z$  are radial and axial (flow) direction. Because  $\tau_{rz}$  is finite with  $r$  approaches 0, solving Equation (1) gives

$$\tau_{rz} = \frac{\Delta P}{2L} r \quad (2)$$

with  $\Delta P$  and  $L$  corresponding to the driven pressure and length of the 3D printing needle, respectively.

Applying Herschel-Bulkley model to express the shear stress, we have

$$\tau_{rz} = \tau_y + K \left( -\frac{\partial u_z}{\partial r} \right)^n \quad (3)$$

The negative sign inside the bracket in Equation (3) reflects that  $\frac{\partial u_z}{\partial r} < 0$  in pipe flows. This means the pipe flow involves two layers along the radial direction as shown in **Figure S9**. In the inner layer, shear stress of the ink is smaller than its yield stress  $\tau_y$  so the ink moves as a whole body ( $\partial u_z / \partial r = 0$ ). And the radius of this layer  $r_0$  is estimated as

$$\frac{\Delta P}{2L} r_0 = \tau_y \quad (4)$$

In the outer layer, however, the ink is yielded and flows like a liquid. Combining Equations (2) and (3) gives

$$\frac{\Delta P}{2L} r = \tau_y + K \left( -\frac{\partial u_z}{\partial r} \right)^n \quad (5)$$

that is subject to the no-slip boundary condition at the needle wall  $u_z = 0 @ r = R$ . This leads to the expression of velocity distribution in the outer layer

$$u_z = \frac{2n}{1+n} \frac{K}{\Delta P/L} \left[ \left( \frac{\Delta P}{L} \frac{R}{2K} - \frac{\tau_y}{K} \right)^{\frac{n+1}{n}} - \left( \frac{\Delta P}{L} \frac{r}{2K} - \frac{\tau_y}{K} \right)^{\frac{n+1}{n}} \right] \quad (6)$$

from which the uniform flow velocity in the inner layer is given by  $u_z @ r = r_0$ , i.e.,

$$u_z^{inner} = \frac{2n}{1+n} \frac{K}{\Delta P/L} \left( \frac{\Delta P}{L} \frac{R}{2K} - \frac{\tau_y}{K} \right)^{\frac{n+1}{n}} \quad (7)$$

The extrusion velocity of KNF-PVA ink is the cross-sectional average of  $u_z$  including the inner and outer layers,

$$\bar{u}_z = \frac{(\pi r_0^2 u_z^{inner} + \int_{r_0}^R 2\pi r u_z dr)}{\pi R^2} \quad (8)$$

Substituting fitted rheological properties ( $\tau_y$ ,  $K$ ,  $n$ ) from **Figure S8** and geometrical parameters of the 3D printing needle ( $L = 1.3$  cm,  $R = 250$   $\mu$ m), we can calculate  $\bar{u}_z$  at different driving pressure  $\Delta P$  as shown in **Figure S10**.

## 2. Supplementary figures

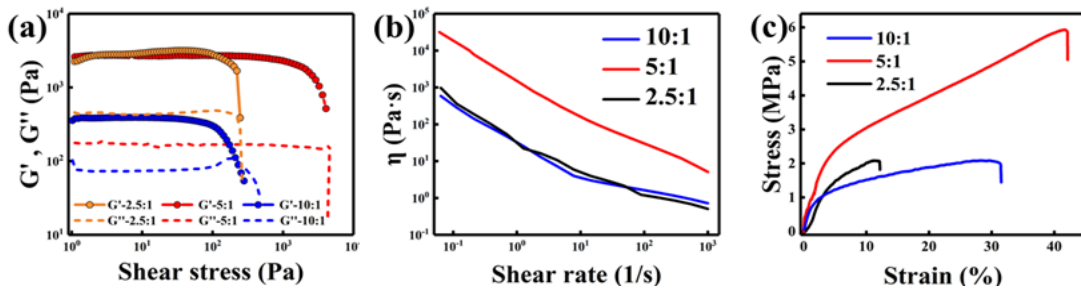


**Figure S1.** Rheological and mechanical properties of 4%-KNF-PVA inks of different PVA:KNF ratio at 2.5:1, 5:1, and 10:1. (a) Storage ( $G'$ ) and loss ( $G''$ ) modulus versus shear stress. (b) Shear rate dependent viscosity. (c) Tensile-stress curve of KNF-PVA aerogel.

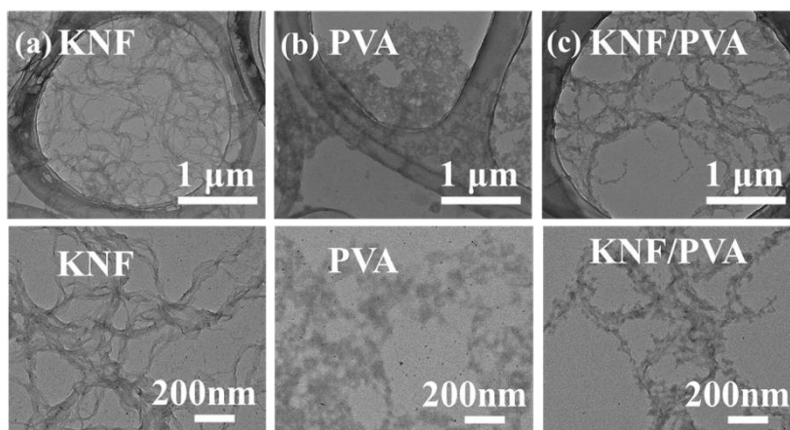


**Figure S2.** TEM images of KNF, PVA, KNF-PVA dispersed in DMSO.

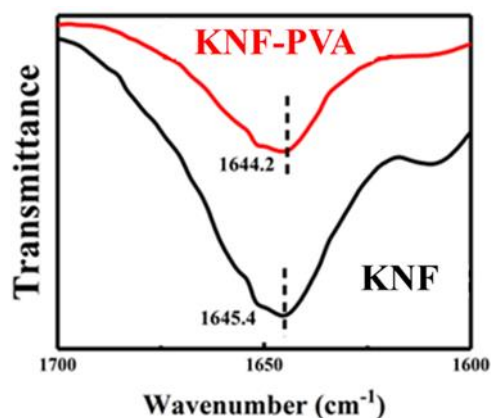


**Figure S3.** Redshift of the C=O stretching vibration peak in FTIR spectrum of KNF-PVA and KNF samples.

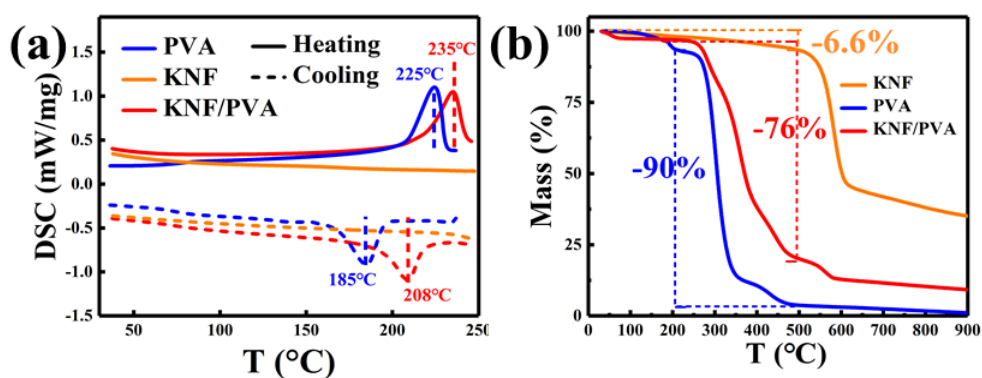


**Figure S4.** DSC (a) and TGA (b) curves of PVA, KNF, and KNF-PVA.

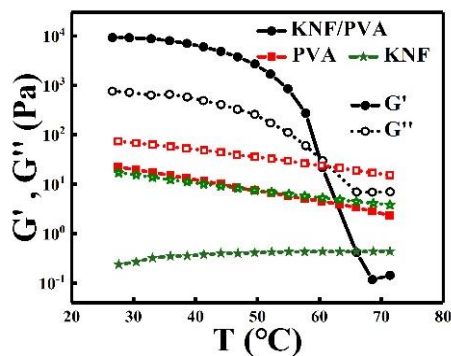


**Figure S5.** Storage ( $G'$ ) and loss ( $G''$ ) modulus versus temperature for DMSO solutions of 2 wt.% KNF, 10 wt.% PVA and 6 wt.% KNF-PVA.

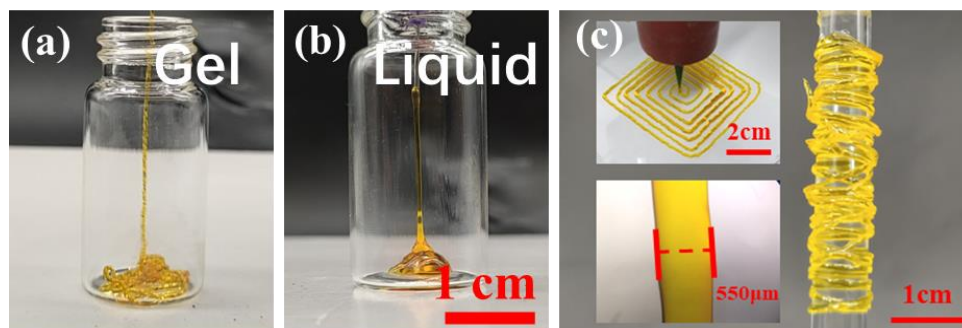


**Figure S6.** Photographs of 3D printing 4%-KNF-PVA inks using printing needle of diameter 500  $\mu\text{m}$ . (a) gel state (45  $^{\circ}\text{C}$ ), (b) liquid state (55  $^{\circ}\text{C}$ ), (c) continuous printing of lines with diameters around 550  $\mu\text{m}$ , within 10% variation from printing needle diameter.

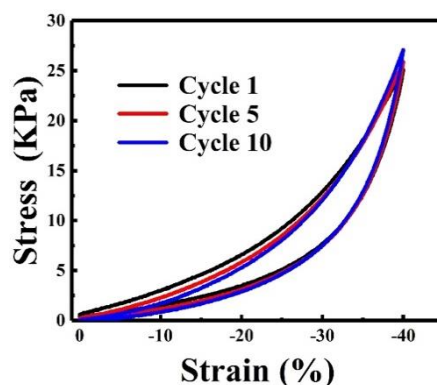


**Figure S7.** Ten repeated compression-relaxation stress-strain curves of 6% KP-I.

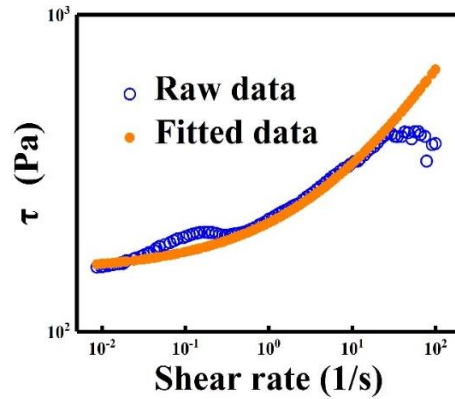


**Figure S8.** Fitting the shear stress vs shear rate curve following the Herschel-Bulkley model shown as Equation (3) in the main text for 4%-KNF-PVA ink characterized at 45 °C. From the fitting,  $\tau_y = 155.5$  Pa,  $K = 65.2$  Pa  $\cdot$  s $^{\frac{1}{n}}$  and  $n = 0.45$ .

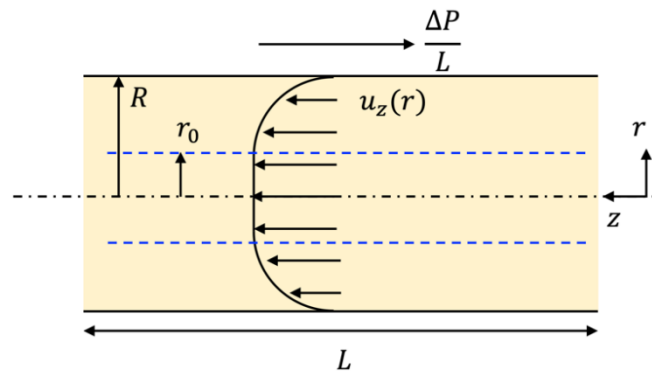


**Figure S9.** Schematic diagram of pressure-driven flow of KNF-PVA inks in the printing nozzle. The flow profile involves two regions: in the inner region  $r < r_0$  the KNF-PVA ink is unyielded and flows as a whole body ( $\frac{\partial u_z}{\partial r} = 0$ ), and in the outer region the ink is yielded by the shear stress and the distribution of velocity follows Equation (6). No slip boundary ( $u_z = 0$ ) is applied at the wall and velocity is continuous at the boundary between inner and outer region.

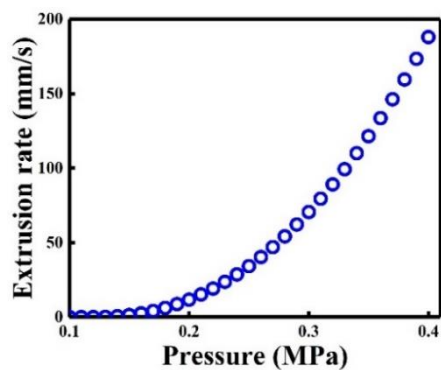


**Figure S10.** Extrusion rate of ink calculated at different driving pressure.

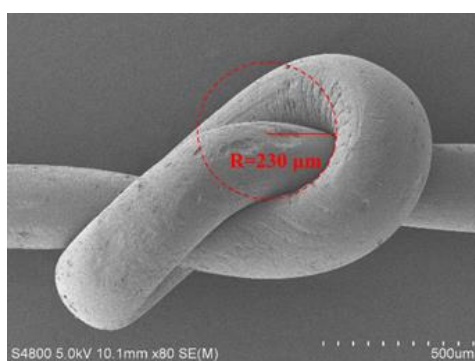


**Figure S11.** Curvature of radius characterized for 3D-printed 4%-KNF-PVA aerogel.

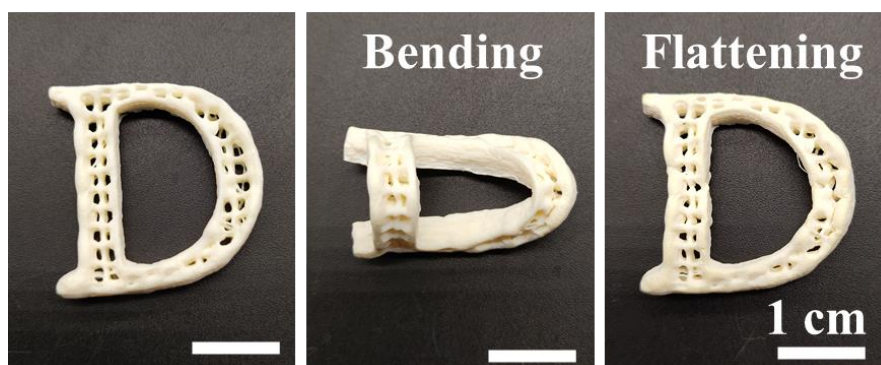


**Figure S12.** Flexibility of the 3D-printed 4%-KNF-PVA aerogel.

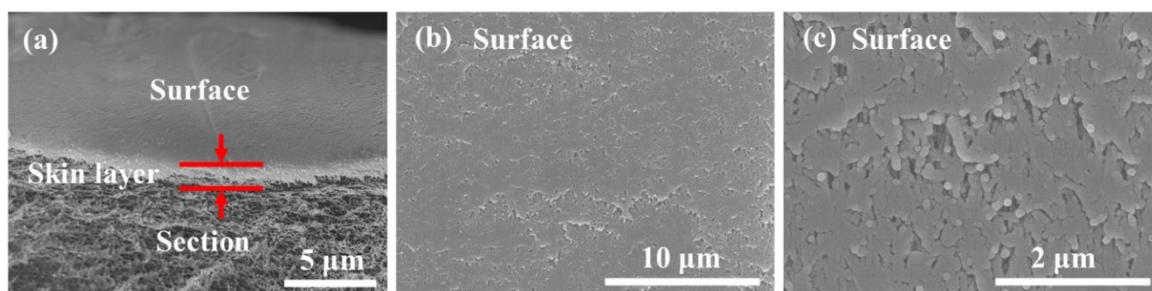


**Figure S13.** SEM images of surface morphology of the hydrogel prepared by immersing liquid KNF-PVA ink in water. (a) side view, (b) top view, (c) zoomed-in details of dense surface. The red arrows in (a) indicated the dense skin layer on the aerogel surface due the outward diffusion of KNF and subsequent cross-linking at the surface.

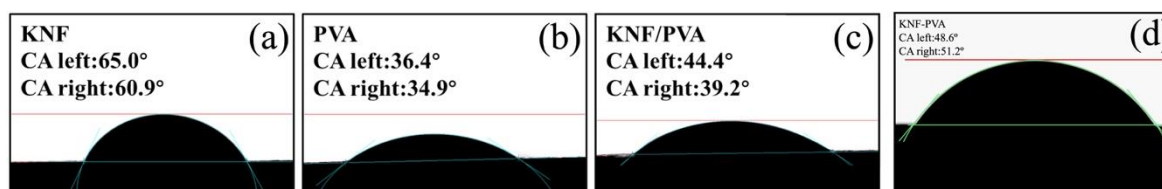


**Figure S14.** The apparent contact angle of water on (a) KNF, (b) PVA, (c) KNF-PVA samples and (d) fresh blood from the Sprague-Dawley rat (as used for in-vitro tests) on KNF-PVA aerogel gauzes.

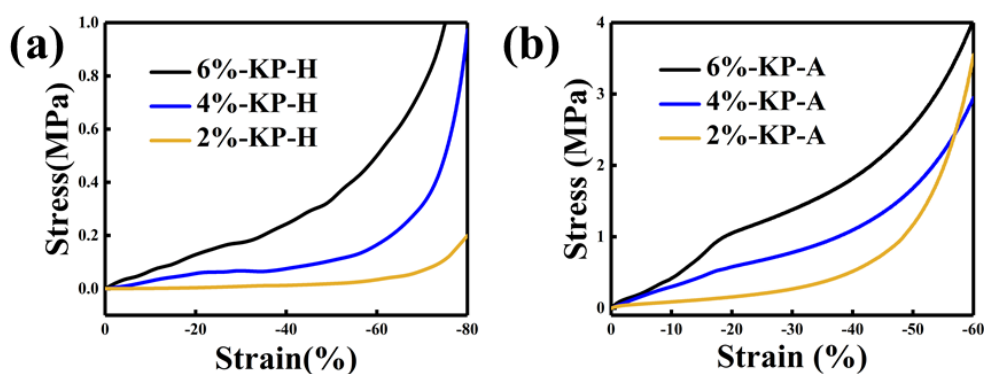


**Figure S15.** Stress–strain curves for hydrogel (a) and aerogel (b) of the same total concentration of KNF and PVA.



**Figure S16.** Photograph showing 4%-KNF-PVA aerogel withstanding the compression from 1 Kg weight.

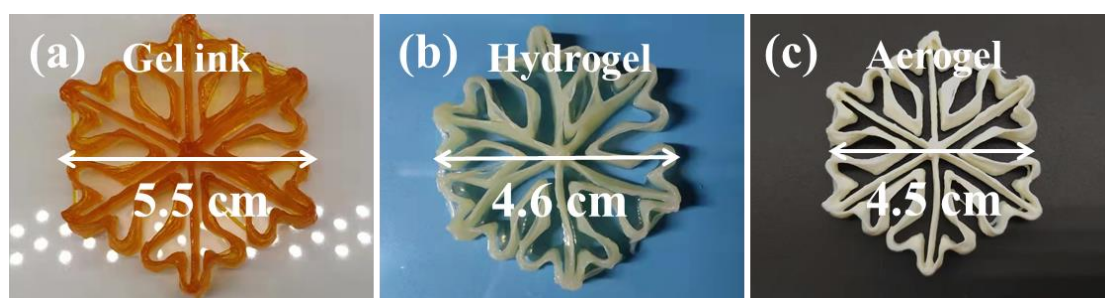


**Figure S17.** Dimensional changes during the preparation of 3D-printed KNF-PVA aerogel from (a) gel ink, (b) hydrogel, and (c) aerogel.

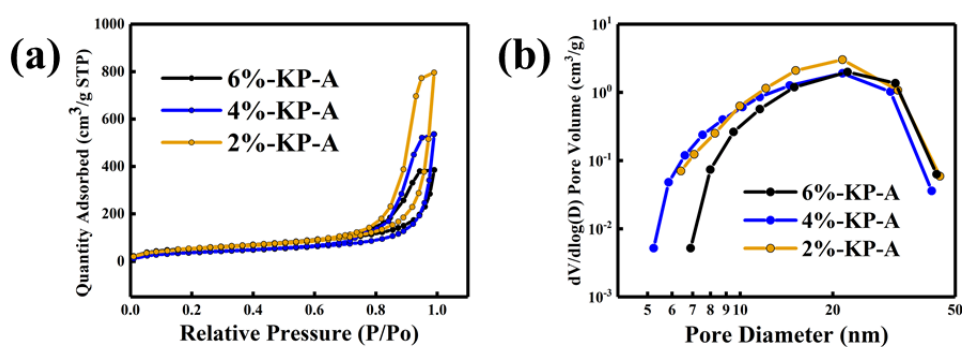


**Figure S18.** (a) Nitrogen adsorption–desorption isotherm and (b) pore volume distribution of KNF-PVA aerogels of different total concentration.

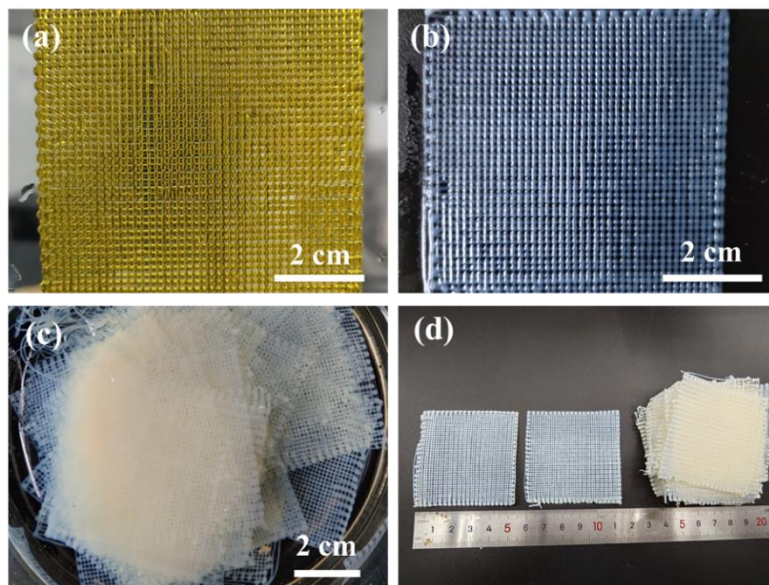


**Figure S19.** Preparation of 3D-printed aerogel gauze. (a) 3D printed gauze with KNF-PVA inks (in DMSO), (b) hydrogel gauze after exchanging DMSO by water, followed by exchanging water with ethanol, (c) high throughput solvent exchange operation, (d) comparison of aerogel gauze's dimensions after supercritical drying (left), after solvent exchange (middle), after 3D printing (right).

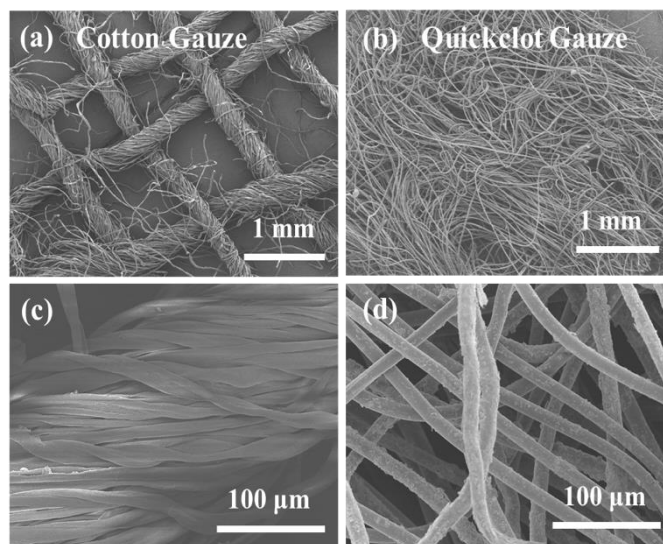


**Figure S20.** SEM images of (a & c) surgical cotton gauze and (b & d) commercial gauze Quickclot Gauze (QCG).

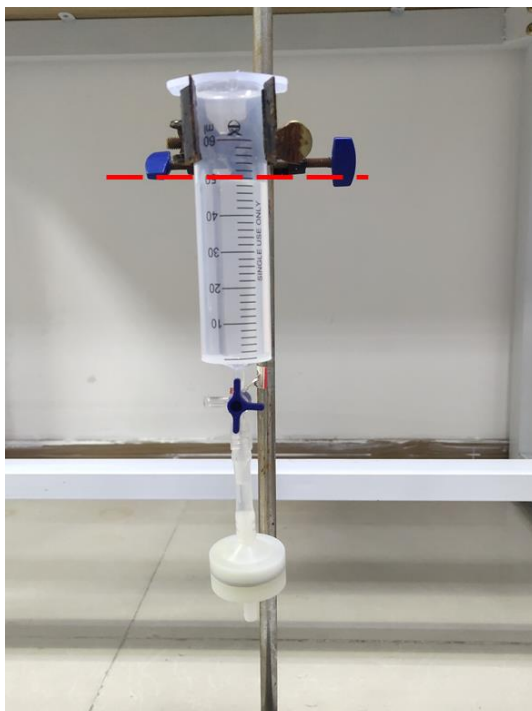


**Figure S21.** Water cannot permeate KNF-PVA aerogel film (thickness 200  $\mu\text{m}$ ) without applying pressure. The aerogel film is enclosed in the film holder with open area of 0.95  $\text{cm}^2$ , and the dashed line indicates the water level ( $\sim 50$  mL) in the syringe.

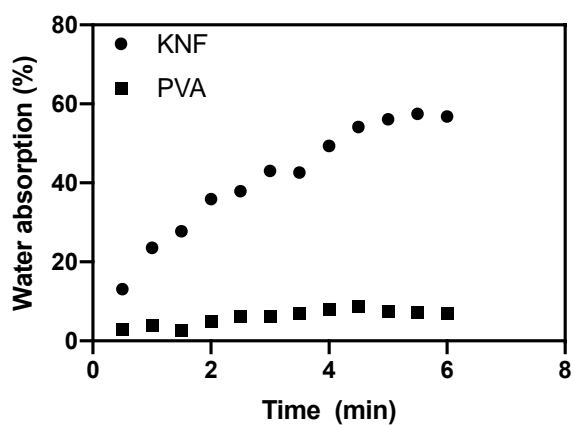


**Figure S22.** Water absorption of KNF and PVA samples.

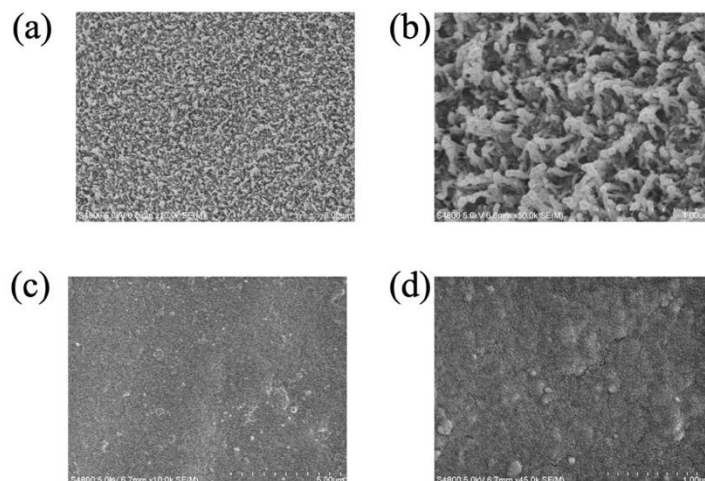


**Figure S23.** SEM characterization of KNF (a-b) and PVA (c-d) samples that were tested for their water absorption as shown in **Figure S22**.

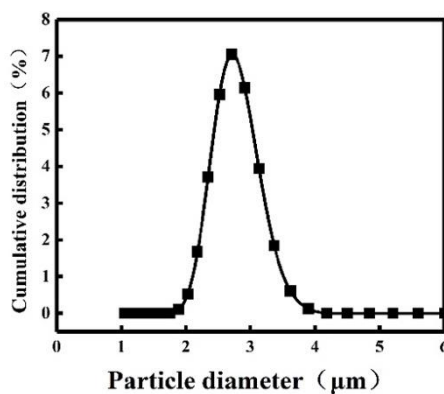


**Figure S24.** The particle size distribution of SiO<sub>2</sub> microspheres used for particle enrichment experiments shown in **Figure 3h**. Preparation of silica microparticles was described in detail in our previous work<sup>1</sup>. Briefly, 5 ml condensed silica solutions were diluted by 5 mL ethanol, then 0.5 mL ammonium hydroxide was added and stirred for 2 min, alcogel formed after standing still for 2 min. The alcogel was aged at 80 °C for 2 h and pulverized by Planetary Ball Mill to obtain uniformly sized SiO<sub>2</sub> microspheres. Such microspheres were soaked in the hexane solution of Sudan-III and dried in oven for staining.

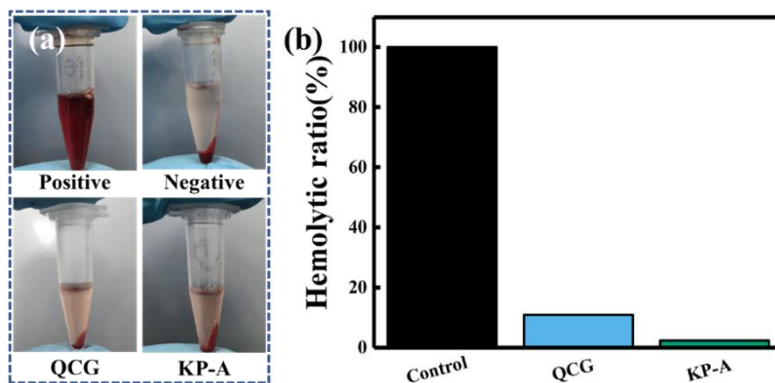


**Figure S25.** Hemolysis rate test. (a) supernatant status after centrifugation, (b) calculated hemolysis rate of different samples.

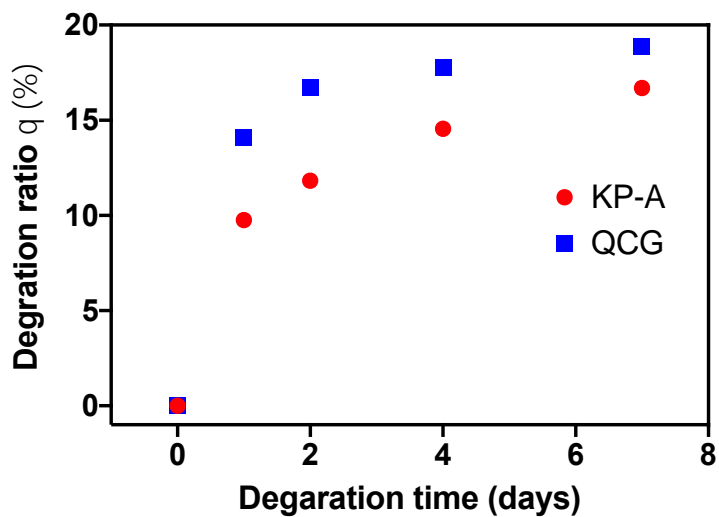


**Figure S26.** In-vitro degradation test of QCG and KP-A.

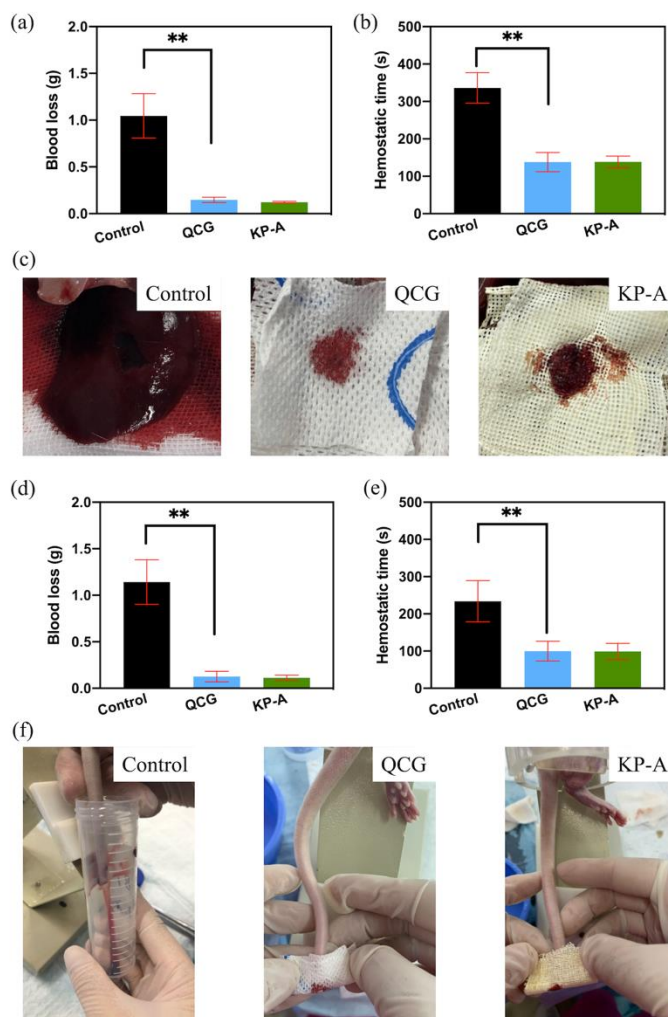


**Figure S27.** In-vivo animal experiments with the rat liver resection and tail amputation model. The rat liver resection model is prepared by resecting a 5 mm long, 5 mm wide, and 5mm deep volume on the left lobe of the rat liver. The rat-tail amputation model is prepared by cutting off the rat tail at 1-2 cm from the tail tip. Comparison of (a) hemostatic time and (b) total blood loss of liver resection wounds with natural hemostasis and applying QCG and aerogel gauzes KP-A. (d) and (e) compare the blood loss and hemostatic time of rat tail amputation wound with natural hemostasis and applying QCG and aerogel gauzes KP-A. (c) and (f) are snapshots showing natural hemostasis and applying hemostatic gauzes on rat liver resection and tail amputation wounds, respectively. All other details are the same as those employed in rat liver laceration model, such as the surface area of applied QCG or KP-A (2.5 cm by 2.5 cm), number of applied layers (three layers), thickness of single layer (1.0 mm). Data in (a)-(b) and (d)-(e) were shown with mean values and standard deviation from three parallel tests (n=3). One-way analysis of variance (ANOVA) by SPSS software (IBM) was

applied for statistical analysis. \* $p < 0.05$  and \*\* $p < 0.01$  were considered significant and greatly significant difference.

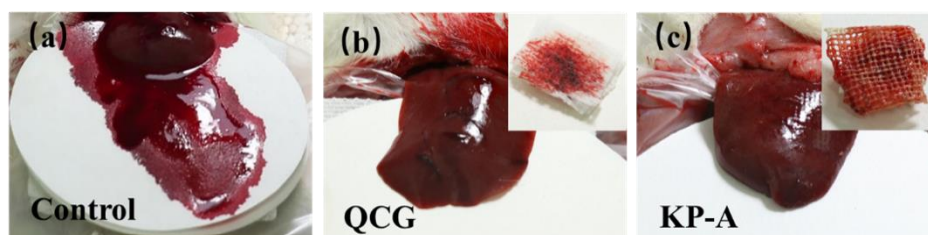


**Figure S28.** Photographs of rat liver wound after (a) natural hemostasis and applying hemostatic materials (b) QCG, (c) KNF-PVA aerogel (KP-A) gauzes.

### 3. Supplementary Tables

**Table S1.** Elastic modulus of KNF-PVA hydrogels and aerogels (corresponding to curves in Figure 3i).

Elastic modulus	Hydrogels	Aerogels
6%-KP	6.16 MPa	111.15 MPa
4%-KP	2.19 MPa	51.31 MPa
2%-KP	1.36 MPa	14.13 MPa

**Table S2.** Specific surface area of aerogels prepared by 3D printing inks of different concentrations in the gel and liquid state.

BET of sample	6%-KP-A	4%-KP-A	2%-KP-A
Liquid ink	111.10 $\text{m}^2 \cdot \text{g}^{-1}$	129.33 $\text{m}^2 \cdot \text{g}^{-1}$	155.47 $\text{m}^2 \cdot \text{g}^{-1}$
Gel ink	111.12 $\text{m}^2 \cdot \text{g}^{-1}$	137.23 $\text{m}^2 \cdot \text{g}^{-1}$	189.01 $\text{m}^2 \cdot \text{g}^{-1}$

**Table S3.** Compression modulus of KNF-PVA hydrogels and aerogels calculated from curves shown in Figure S15.

Compression modulus	Hydrogels	Aerogels
---------------------	-----------	----------

6%-KP	0.84 MPa	7.47 MPa
4%-KP	0.23 MPa	3.53 MPa
2%-KP	0.01 MPa	2.58 MPa

**Table S4.** Specific surface area, porosity and density of aerogels with different total KNF-PVA concentration based on characterization curves in **Figure S18**.

Sample	BET ( $\text{m}^2 \cdot \text{g}^{-1}$ )	Density ( $\text{g} \cdot \text{cm}^{-3}$ )	Porosity (%)
6%-KP	111.12	0.1195	91.01
4%-KP	137.23	0.1034	92.22
2%-KP	189.01	0.0856	93.56

**Table S5.** Theoretical and measured water absorption of aerogel gauzes. Theoretical values are estimated with the density and porosity shown in **Table S1**.

Sample	Theoretical water absorption %	Actual water absorption %
6%-KP	762	725±40
4%-KP	892	888±33
2%-KP	1093	1139±89

#### 4. Supplementary references

- (1) Liu, R.; Wang, J.; Du, Y.; Liao, J.; Zhang, X.; Phase-separation induced synthesis of superhydrophobic silica aerogel powders and granules. *J. Solid State Chem.* **2019**, 279, 120971.